Heliyon 7 (2021) e07466

Contents lists available at ScienceDirect

Heliyon

journal homepage: www.cell.com/heliyon

Research article

Mathematical modeling and stochastic simulations suggest that low-affinity peptides can bisect MHC1-mediated export of high-affinity peptides into "early"- and "late"-phases

Siddhartha Kundu *

Department of Biochemistry, All India Institute of Medical Sciences, Ansari Nagar, New Delhi – 110029, India

ARTICLE INFO

Keywords:
Low-affinity peptides
Major histocompatibility complex
Peptide loading complex
PLC-assembly/disassembly
Peptide editing
Shunt reaction
Stochastic simulation algorithm
Tapasin

ABSTRACT

The peptide loading complex (PLC) is a multi-protein complex of the endoplasmic reticulum (ER) which optimizes major histocompatibility I (MHC1)-mediated export of intracellular high-affinity peptides. Whilst, the molecular biology of MHC1-mediated export is well supported by empirical data, the stoichiometry, kinetics and spatio-temporal profile of the participating molecular entities are a matter of considerable debate. Here, a low-affinity peptide-driven (LAPD)-model of MHC1-mediated high-affinity peptide export is formulated, implemented, analyzed and simulated. The model is parameterized in terms of the contribution of the shunt reaction to the concentration of exportable MHC1. Theoretical analyses and simulation studies of the model suggest that low-affinity peptides can bisect MHC1-mediated export of high-affinity peptides into time-dependent distinct "early"- and "late"-phases. The net exportable MHC1 ($eM1\beta(t)$) is a function of the retrograde ($rM1\beta(t)$)- and anterograde ($aM1\beta(t)$)-derived fractions. The "early"-phase is dominated by the contribution of the retrograde/recyclable ($rM1\beta \approx 61\%, aM1\beta \approx 39\%$) pathway to exportable MHC1, is characterized by Tapasin-mediated peptide-editing and is ATP-independent. The "late"-phase on the other hand, is characterized by *de novo* PLC-assembly, rapid disassembly and a significant contribution of the anterograde pathway to exportable MHC1 ($rM1\beta \approx 21\%, aM1\beta \approx 79\%$). The shunt reaction is rate limiting and may integrate peptide translocation with PLC-assembly/disassembly thereby, regulating peptide export under physiological and pathological (viral infections, dysplastic alterations) conditions.

1. Introduction

The major histocompatibility complex (MHC), is a clustered group of cell surface proteins that participates in the adaptive immune response and is present in most vertebrates [1, 2, 3, 4, 5, 6, 7, 8, 9]. These genes, in humans ($n = 240$), are also known as human leukocyte antigens (HLA) and are present on the short arm of chromosome 6 ($6p21.3 - 6p22.3$) (**Fig. 1a**). In contrast, the minor histocompatibility proteins (MiHA) are smaller ($9 - 12$ *aa*) and occur in genes which exhibit polymorphisms [10, 11, 12, 13]. Proteins of the MHC have been ascribed roles in the endogenous- (MHC class I), exogenous- (MHC class II), and cross-processing pathways of peptide immunogens (**Figs. 1b and 1c**) [6, 14, 15, 16, 17, 18, 19, 20, 21, 22, 23, 24]. The ubiquitously present MHC class I proteins present peptides to CD8+ cytotoxic T-cells and are derived from cells infected with intracellular pathogens or undergoing dysplastic alteration(s) (**Figs. 1a and 1b**) [6, 17, 20, 23]. In contrast, immunogens derived from extracellular pathogens are internalized and processed by MHC class II proteins in the endoplasmic reticulum (ER) of professional antigen presenting cells (APC) *en route* to being presented to CD4+ helper T-cells (**Figs. 1a and 1c**) [24]. The miscellaneous MHC class III proteins partake in processing immunogens via the complement pathway(s) (C2, C4, B-factor) and function as cytokines (tumor necrosis factor-α, leukotrienes -A and -B) or heat shock proteins (**Fig. 1a**) [25, 26, 27, 28, 29]. The proteome fingerprint of an altered cell is distinct from neighboring cells and may serve as a molecular flag of infection or impending cellular alteration (**Fig. 1**) [14, 15, 16, 17, 18, 21, 22, 24].

The peptide loading complex (PLC), is a transient complex of several ($n \geq 5$) proteins and functions to translocate and thence load cytosolic peptides onto newly synthesized MHC1 in the lumen of the ER [30, 31, 32, 33, 34, 35]. The molecular participants of the PLC comprise the

* Corresponding author.
E-mail addresses: siddhartha_kundu@yahoo.co.in, siddhartha_kundu@aiims.edu.

https://doi.org/10.1016/j.heliyon.2021.e07466
Received 8 March 2021; Received in revised form 23 May 2021; Accepted 29 June 2021

a.

Complex	HLA – HUMAN LEUKOCYTE ANTIGEN; Chromosome 6p							
Class	II			III		I		
	Classical					*Classical*		
Locus	DP	DQ	DR	C2, C4, BF		B	C	A
Products	HLA-DP	HLA-DQ	HLA-DR			HLA-B	HLA-C	HLA-A
	Non classical			C'	TNF-α,-β	*Non classical*		
Locus	DM, DO					E, F, G, H		
Products	HLA-DM, -DO					HLA-E, -F, -G, -H		

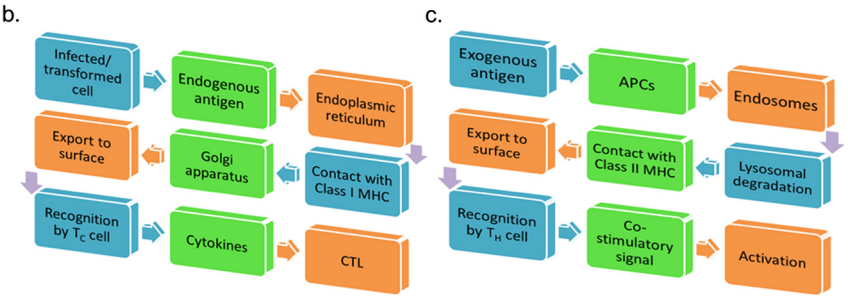

Fig. 1. Salient features of the human MHC complex. a) The MHC complex in humans (HLA) is a cluster of loci ($n \cong 240$) and is present on the short arm of chromosome 6 ($6p$). The encoded proteins are classified as classical and non-classical/atypical, b) Class I restriction of cytotoxic T-cells ($CD8+$) is brought about when the heterodimer of MHC1 and β_2-microglobulin in the ER of a nucleated cell presents peptides processed by the ubiquitin-proteasome system to cytotoxic T-cells. The proteins degraded may be physiological or result when cells are infected with cytosolic pathogens or are undergoing dysplastic alterations. This "endogenous" pathway is mediated by the sequential assembly and disassembly of the PLC followed by export to the cell surface, and c) Class II restriction of helper T-cells ($CD4+$), in contrast, occurs in professional antigen presenting cells. Here, MHC class II molecules are loaded with peptides derived from proteins degraded by lysosomal hydrolases. The complex is then transported by endosomes to the cell surface of professional APCs and thence to helper T-cells. **Abbreviations**: **APC**, Antigen presenting cell; **CD**, Cluster designation; **ER**, endoplasmic reticulum; **HLA**, Human leukocyte antigen; **MHC**, major histocompatibility antigen.

transporter(s) associated with antigen processing ($TAP1/2 \equiv$\{TAP1,TAP2\}), Tapasin, ERp57, one or more chaperone proteins, and the MHC class I protein(s) in complex with β_2-microglobulin ($M1\beta$) [30]. The transmembrane (TM)-domain of Tapasin or TAP-associated glycoprotein, associates concomitantly with $TAP1/2$, ERp57 and $M1\beta$ [30]. Tapasin is integral to PLC-assembly and has also been shown to facilitate peptide-editing, i.e., the competitive binding and exchange of peptides with incremental affinities for $M1\beta$ (**Fig. 2**) [30, 31, 32, 36, 37, 38, 39, 40]. ERp57 or protein disulfide-isomerase A3 (PDIA3) (EC 5.3.4.1), utilizes two catalytic ($'CGHC' = \{a, a'\}$) and lysine-rich binding (b, b') domains along with several non-specific protein-protein interactions in forming an extensive contact surface with Tapasin [41, 42, 43, 44, 45, 46, 47, 48, 49, 50]. Whilst, the association of Tapasin and ERp57 is critical to the assembly of the PLC, the inclusion of $M1\beta$ completes its formation [36, 41, 46, 47, 48, 49, 51, 52, 53, 54]. The role of a non-ERp57 Protein disulfide isomerase (PDI) has been shown to effect this process as well, although the mechanism by which it does so, and indeed the presence of it as well has been the subject of much debate [50, 52, 55].

The simplicity of the canonical model of PLC ($TAP1/2 : Tapasin : ERp57 : M1\beta :: 4 : 8 : 4 : 4$) notwithstanding, MHC1-mediated peptide export comprises several interleaved steps [35, 56]. These include: a) ubiquitin-proteasome system (UPS)-mediated intra-cellular protein degradation, b) peptide-affinity dependent PLC-disassembly and c) peptide editing (**Fig. 2**) [30, 31, 32, 56, 57, 58, 59, 60, 61, 62, 63]. Briefly, UPS-derived cytosolic peptides bind $TAP1/2$ and enter the ER lumen by an ATP-dependent and Tapasin-facilitated translocation across the ER membrane [57, 58]. PLC-disassembly is then triggered by the autocatalytic $\left(C406_{ERp57} + C95_{Tapasin} - C57_{ERp57} \rightarrow \left[C406_{ERp57} \cdots C95_{Tapasin} - C57_{ERp57}\right] \rightarrow C406_{ERp57} - C95_{Tapasin} + C57_{ERp57}\right)$ reduction of a disulfide ($-SS-$) linkage between Tapasin and ERp57 [41, 46]. A high-affinity peptide bound to $M1\beta$ will result in immediate disengagement from the PLC with subsequent transport via the Golgi apparatus to the plasma membrane (anterograde pathway) (**Fig. 2**) [46, 59, 60, 61]. On the other hand, a low-affinity peptide, whence bound to $M1\beta$, is incorporated along with Tapasin into COPI-coated vesicles and recycled back to the ER (retrograde pathway) (**Fig. 2**) [46, 62]. The complex kinetics of MHC1-mediated export of high-affinity peptides results in several interesting empirical observations. These include redox regulation, protein-protein interactions and peptide editing (**Fig. 2**) [30, 31, 45, 55]. The latter is particularly relevant given that high-affinity peptides are present at concentrations much lower that low-affinity variants. Here, too, Tapasin is a major contributor although, the manner in which it does so is speculative [39, 40].

Although the underlying molecular biology of MHC1-mediated export of high-affinity peptides is well understood, mechanistic details (stoichiometry, kinetics, spatio-temporal profiles) of the participating molecular entities are unclear. In this study, the regulatory influence of low-affinity peptides on MHC1-mediated adaptive immunosurveillance is explored via the shunt reaction and peptide editing [39, 40]. This is accomplished by formulating, implementing and analyzing a low-affinity peptide-driven (LAPD)-model of MHC1-mediated peptide export. The detailed theoretical analyses will be complemented by stochastic simulations of the model. Stochastic simulations, unlike ordinary (ODE)- and partial-differential (PDE)-equation based kinetic modeling are accurate and unbiased in their approximation of the chemical master equation (CME). However, this also implies that inferring meaningful information from the raw data *post hoc*, will mandate considerable pre-processing. Initial simulations will be conducted to parameterize the steady state of the LAPD-model of exportable MHC1. The resulting datasets will be extensively parsed for time-step matched concentrations of the molecules and analyzed by regression $\left(\text{timestep}\sim\text{molecule}, \text{molecule}\sim\text{molecule}\right)$ models. These data will then be utilized in later simulations to establish a temporal profile of the molecular entities and the complexes that they partake in.

The manuscript comprises a "Methods"-section, where a generic representation of a closed set of reactions and the numerical approximation of their solutions is given as a rationale for this study. Additionally, the section also highlights the modeling strategy deployed, tools and numerical methods needed to process the data that results from the simulations. This is followed by the "Results"-section where the definition and formulation of the LAPD-model, notations, derivations of the CME of net exportable MHC1 and preliminary results of the underlying molecular biology of

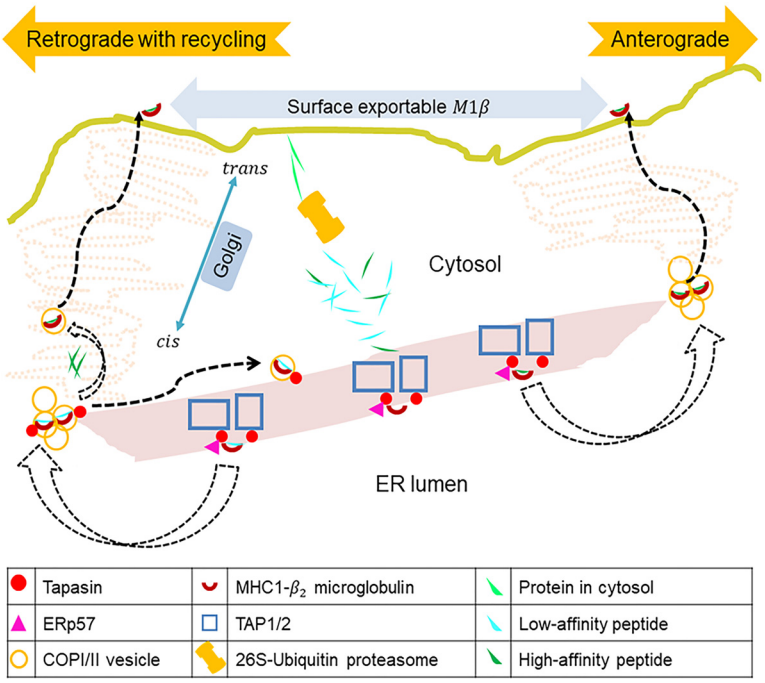

Fig. 2. Cell and molecular biology of MHC1-mediated peptide export. Cytosolic peptides from routine proteolysis, cells undergoing dysplastic alterations, and infections with intra-cytoplasmic pathogens are derived after they are degraded by the 26S-Ubiquitin-proteasome system. These enter the ER-lumen by an ATP-dependent and $TAP1/2$-mediated translocation across the ER membrane. The peptide loading complex is a multi-protein complex that loads MHC1 molecules with peptides. PLC-disassembly is bimodal and comprises the anterograde- and retrograde-pathways. This bifurcation depends on the affinity of peptides for MHC1 (peptide editing) and Tapasin's concomitant interactions with ERp57 and $M1\beta$. Whilst, high-affinity peptides are exported via the anterograde route ($COPII \rightarrow cis\ Golgi \rightarrow trans\ Golgi \rightarrow cell\ membrane$), low-affinity variants are recycled back by the retrograde ($COPI \rightarrow cis\ Golgi \rightarrow ER$) pathway. **Abbreviations**: **COP**, coatomer protein; **Cx**, chaperone proteins (Calreticulin/Calnexin); ***K***, Lysine; MHC1, major histocompatibility 1 antigen; **PLC**, set of differential forms of the peptide loading complex; ***TAP1/2***, transporters associated with antigen processing; **UPS**, ubiquitin-proteasome system.

MHC1-mediated export of high-affinity peptides are given. Finally, these results are "Discussed" in context of the patho-physiological relevance of low-affinity peptides and Tapasin in the regulation of MHC1-mediated export of intracellular high-affinity peptides to the plasma membrane. A final section, "Conclusions" summarizes the main findings, limitations and future directions of this work.

2. Methods

2.1. Modeling strategy and rationale

The modeling approach adopted in this manuscript is the numerical approximation of a chemical master equation (CME) of net exportable MHC1 by Gillespie's stochastic simulation algorithm (SSA) [64, 65]. Here, the model is a closed well-mixed set of inter-dependent non-enzymatic reactions of the investigated molecular entities. This results in a system whose products are generated and utilized in accordance with their computed propensities.

Consider an arbitrary system of molar concentration of reactants (A-D) and reactions that they participate in. The reactions are non-enzymatic and paired (forward, backward) with rate constants (k_f, k_b) in terms of a disassociation (K_d) constant, i.e., $K_d \approx \frac{k_f}{k_b}$.

$$
\begin{array}{lllllll}
[A] & + & [B] & \rightarrow & [AB] & & \textit{Reaction } 1 \\
 & & [AB] & \rightarrow & [A] & + [B] & \textit{Reaction } 2 \\
[A] & + & [C] & \rightarrow & [AC] & & \textit{Reaction } 3 \\
 & & [AC] & \rightarrow & [A] & + [C] & \textit{Reaction } 4 \\
[C] & + & [D] & \rightarrow & [CD] & & \textit{Reaction } 5 \\
 & & [CD] & \rightarrow & [C] & + [D] & \textit{Reaction } 6
\end{array}
$$

The equations to determine the molar concentration of [A] at any instant of time are then,

$$[\dot{A}] = k_2([AB]) + k_4([AC]) - k_1([A][B]) - k_3([A][C]) \quad (1)$$

$$[\dot{B}] = k_2([AB]) - k_1([A][B]) \quad (2)$$

$$[\dot{C}] = k_6([CD]) - k_5([C][D]) \quad (3)$$

$$[\dot{D}] = k_6([CD]) - k_5([C][D]) \quad (4)$$

$$[\dot{AB}] = k_1([A][B]) - k_2([AB]) \quad (5)$$

$$[\dot{CD}] = k_5([C][D]) - k_6([CD]) \quad (6)$$

Table 1. Constraints and parameters utilized to model and simulate the LAPD-model of MHC1-mediated export of high affinity peptides.

S. No.	Name	Parameter	Quantity
1	Range of numerical values utilized for disassociation constants	K_d	$[10^{-6}, 1.00]$
2	Proportion of empirically observed MHC1	$\frac{[eM1\beta]}{[rM1\beta]}$	≈5.00
3	Fold difference between low- and high-affinity peptides	$Log\left(\frac{\#Lp}{\#Hp}\right)$	≈5.00
4	Rate limiting step (shunt reaction)	k_{18}	$30-35\ \mathrm{mol\,L^{-1}\,s^{-1}}$
5	Total number of reactions	RXN	30
	Total number of forward reactions	RXN_f	15
	Total number of backward reactions	RXN_b	15
6	Index of molecular entity	i	18
7	Number of *in silico* experiments	j	3
8	Number of independent runs or observations	h	30
9	Number of molecules of an entity per *in silico* experiment in an independent run or observation	y_{ijh}	—
10	Wall time of each independent run or observation	—	600 s
11	Time units	tf	100
12	Degree of freedom	df	28
13	Simulation time to assess temporal variation of molecular entity	t	[60 s, 900 s]

The solutions of these equations can be incorporated into the equation (1) along with the substitution,

$$k_3([A][C]) = k_6([CD]) - k_5([C][D]) \tag{7}$$

to generate a composite CME for $[A]$,

$$\begin{aligned}[B] &= \int \left(k_2([AB]) - k_1([A][B])\right) dt \\ &= k_2([AB]) - k_1([A][B]) + c_{[AB]}\end{aligned} \tag{8}$$

$$\begin{aligned}[C] = [D] &= \int \left(k_6([CD]) - k_5([C][D])\right) dt \\ &= k_6([CD]) - k_5([C][D]) + c_{[CD]}\end{aligned} \tag{9}$$

$$\begin{aligned}[A] &= \int \left(k_2([AB]) + k_4([AC]) - k_1([A][B]) - (k_6([CD]) - k_5([C][D]))\right) dt \\ &= k_2([AB]) + k_4([AC]) - k_1([A][B]) - \left(k_6([CD]) - k_5([C][D])\right) + c_{[A]}\end{aligned} \tag{10}$$

Here,

$$\begin{aligned}[.] &:= \textit{Molar concentration of reactant}\ (\mathrm{mol\,L^{-1}}) \\ k &:= \textit{Rate constant of reaction}\ (\mathrm{mol\,L^{-1}\,s^{-1}}) \\ c_{[.]} &:= \textit{Arbitrary constant of the solution of the equation for reactant}\end{aligned}$$

Equation (10), which is the net concentration of molecule "A" may then be directly approximated by simulation data.

2.2. Implementing a model of MHC1-mediated peptide export

2.2.1. Constraint-based model of exportable MHC1

MHC1-mediated export of high-affinity peptides is a critical process in the processing and presentation of intracellular immunogens to circulating T- and B-cells. Whilst, there are several excellent manuscripts on individual molecules, the manner in which these work as a cohesive unit *in vivo*, is speculative with several open research problems. This paucity of data is reflected in the absence of usable rate- and stoichiometric-constants of the molecular entities. Here, an *ab initio* constraint-based derivation of the stoichiometric matrix of the molecular participants and the rate constants of reactions that they partake in is undertaken. The primary constraint utilized is the steady state of the modeled system both, at the outset and during simulation runs. This is an essential step in approximating the CME of net exportable MHC1. Other constraints include equivalent and non-limiting initial values of each molecular entity (zero-order kinetics) and bounded rate constants for any arbitrary pair of reactions. The latter are chosen such that the net flux is not more than 6-fold ($10^{-6} < \frac{k_f}{k_b} \approx K_d \leq 1$) (**Table 1**). The rationale for this is that the SSA computes the propensity of occurrence of a particular reaction and any value in excess of this ratio may result in a particular state/reaction occurring more frequently which will bias the system. Additional constraints are based on empirical data, whence available. This includes the proportions of exportable MHC1 and low- and high-affinity peptides (**Table 1**). Since the objective of this work is to study the effect of low-affinity peptides on the shunt reaction and thence the exportable MHC1, the model is parameterized in terms of the same (**Table 1**). The model is implemented in R-3.1.2 and includes in-house coded scripts for controlling the runs, parsing, analyses and processing the resulting data (**Table 1**).

2.2.2. Simulations and numerical approximation of the CME of exportable MHC1

The CME of exportable MHC1 that is formulated *vide infra*, is a complex mathematical expression of several molecular entities (ERp57, Tapasin, low- and high-affinity peptides, MHC1-β_2) and/or their complexes. The major focus of this manuscript is the temporal assessment of the molecules that influence MHC1-mediated export of high-affinity peptides to the plasma membrane. Since the time-step is randomly chosen, a comparative assessment is only possible by imputing a single time-step and thence inferring the number of molecules at that time-step [66]. The initial round of simulations is done to parameterize the steady state of the system. The linear models thus generated along with simulation data from the final

round of simulations will result in a time-based trajectory of each molecular entity. Clearly, this non-standard usage of the SSA mandates a detailed explanation which along with the relevant formulas and equations is outlined. This approach has been successively deployed previously and the data generated was used to glean insights into the vectorial chemotaxis of an advancing phagocyte [66].

Briefly, (h)-independent runs or "observations" comprise a single *in-silico* experiment (j) for an indexed set of molecular entities (i) (**Table 1**). A linear model is then used to associate the run-specific time-step $\left(t_{jh} \in \boldsymbol{T}\right)$ with a numerical estimate of a specific molecular entity $\left(y_{ijh} \in \boldsymbol{Y}\right)$,

$$y_{ijh} \sim t_{jh} \tag{11}$$

This will compute several coefficients such as estimates of standard error, t-value, and the probability of error $(pr > |t - value|)$ of the intercept (λ), slope (θ) and the degree of freedom (df).

$$\left\{\lambda_{yij} \in \mathbb{R}_+ | \lambda_{y_{ij}} = \lambda(y_{ij}) = mean\left(\lambda_{yij1}, \lambda_{yij2}, \ldots . \lambda_{yijh}\right)\right\} \quad y_{ijh} \in \boldsymbol{Y} \tag{12}$$

$$\left\{\theta_{yij} \in \mathbb{R}_+ | \theta_{yij} = \theta(y_{ij}) = mean\left(\theta_{yij1}, \theta_{yij2}, \ldots . \theta_{yijh}\right)\right\} \quad y_{ijh} \in \boldsymbol{Y} \tag{13}$$

Since, the time-steps chosen by the SSA during each run are random the median value $\left(t_j\right)$ for a set of (h)-runs is chosen,

$$\left\{t_j \in \mathbb{R}_+ | t_j = t(j) = median\left(t_{j1}, t_{j2} \ldots \ldots t_{jh}\right)\right\} \quad t_{jh} \in \boldsymbol{T} \tag{14}$$

These parameters are then utilized to impute the time-step invariant quantities of each molecule in a single *in silico* experiment,

$$\left\{\Delta y_{ij} \in \mathbb{R}_+ | y_{ij} = \left(\left(t_j\right)\left(\theta_{yij}\right)\right) + \lambda_{yij}\right\} \tag{15}$$

The temporal variation of an arbitrary molecular entity is then calculated in triplicate $(j \in [1,3])$ using the arithmetic mean (μ) and standard deviation (σ) as numerical indices (**Table 1**). The aforementioned steps are summarized,

$$\begin{pmatrix} y_{i11} & \cdots & y_{i1h} \\ \vdots & \ddots & \vdots \\ y_{ij1} & \cdots & y_{ijh} \end{pmatrix} \rightarrow \begin{matrix} \Delta y_{i1} \\ \vdots \\ \Delta y_{ij} \end{matrix} \rightarrow \left\{\mu\left(\Delta y_{ij}\right), \sigma\left(\Delta y_{ij}\right) | j \in [1,3]\right\}$$

The raw parameterization data (initial simulations) and the temporal variations of the molecular entities observed (final simulations) are included as supplementary material (**Supplementary Tables 1-4, Supplementary Texts 1-4**). Miscellaneous parameters such as console interval and time units are in accordance with the package guidelines (GillespieSSA) and previous work (**Table 1**) [66].

3. Results

Protein-protein interactions (PPI), are the molecular basis for PLC assembly/disassembly and may have a significant role in the export of high-affinity peptides by MHC1 to the plasma membrane [30, 31, 32, 33]. The PLC is a large macromolecular complex and is arguably the most important component of MHC1 $(M1\beta)$-mediated antigen processing and presentation of intracellular immunogens (**Fig. 2**). Similarly, the ternary complex of Tapasin and low-affinity peptide bound $M1\beta$ $\left(PPI_{Tapasin-M1\beta Lp}\right)$, represents the exchangeable fraction of MHC1 and is a key determinant of peptide editing (**Fig. 2**). Other notable complexes of physiological relevance include Adenosine triphosphate (ATP) with the transporters associated with antigen processing $\left(PPI_{ATP-TAP1/2}\right)$ and the association between ERp57 and Tapasin $\left(PPI_{ERp57-Tapasin}\right)$ (**Fig. 2**).

3.1. Definitions and preliminary results of a model of MHC1-mediated export of high-affinity peptides

The low-affinity peptide-driven (LAPD)-model purports that low-affinity peptides $\left(Lp_n \in \boldsymbol{Lp}, n \in \mathbb{N}\right)$ are significant determinants of the efficient and continuous export of high-affinity peptides $\left(Hp_m \in \boldsymbol{Hp}, m \in \mathbb{N}\right)$ by the MHC1- β_2-microglobulin heterodimer $(M1\beta)$. These definitions are derived from empirical data of the disassociation constants, $K_d(.)$, of these peptides in association with $M1\beta$,

$$Lp_n \equiv K_d\left(M1\beta Lp_n\right) \approx 1.0, \quad Def.(1)$$
$$Hp_m \equiv K_d\left(M1\beta Hp_m\right) \approx 0.0 \quad Def.(2)$$

This implies that higher-order complexes such as the peptide loading complex (PLC) that result from these interactions will exhibit a dual distribution,

$$\left\{PLC_z \in \boldsymbol{PLC} | PLC_z \sim PLC_z Hp_m \vee PLC_z Lp_n\right\} \quad Def.(3)$$

Here, PLC_z is an arbitrary indexed entity from the pool of cytosolic PLC $(\boldsymbol{PLC})$ and can be bound to a high $\left(PLC_z Hp_m\right)$- or low $\left(PLC_z Lp_n\right)$-affinity peptide where, $\{z, m, n\} \in \mathbb{N}$. The joint probability of the simultaneous occurrence of every PLC form $(Prob(\boldsymbol{PLC}))$ may be approximated by the probability mass function of the Binomial Distribution:

$$p = Prob(PLC_z = PLC_z Hp_m) \equiv Prob(Hp_m) = 0.00001 \tag{16}$$

$$q = Prob(PLC_z = PLC_z Lp_n) \equiv Prob(Lp_n) = 0.99999 \tag{17}$$

$$X = Prob(\boldsymbol{PLC}) \sim \binom{s}{r}(p)^r (q)^{s-r} = B(s,p) \tag{18}$$

$$\lim_{s \to \infty} X = \lim_{s \to \infty} B(s,p) \to 0 \forall s > 1 \tag{19}$$

s := *Combined pool of indexed* PLC_z *forms*
r := *Occurrence of* PLC_z *bound high-affinity peptide*
B := *Binomial distribution of cytosolic* $\boldsymbol{PLC}$

Table 2. Low-affinity peptide-driven (LAPD)-model of MHC1-mediated export of high-affinity peptides.

Non-stoichiometric molar representation of molecular entities	k_{RXN} (mol L^{-1} s^{-1})	Molecular Biology		
		PT	PLCa	PLCd
$[\text{Tapasin\_TAP1/2}] + [\text{M1}\beta] \underset{2}{\overset{1}{\leftrightarrow}} [\text{Tapasin\_TAP1/2\_M1}\beta\text{\_ERp57\_Cx/Cr}]$	$k_1 = 1.00,\ k_2 = 10^{-4}$	-	+	-
$[\text{Lp}_n] + [\text{ATP\_TAP1/2}] \underset{4}{\overset{3}{\leftrightarrow}} [\text{ATP\_TAP1/2\_Lp}_n]$	$k_3 = 1.00,\ k_4 = 5.00$	+	+	-
$[\text{Tapasin\_TAP1/2\_M1}\beta\text{\_ERp57\_Cx/Cr}] + [\text{ATP\_TAP1/2\_Lp}_n] \underset{6}{\overset{5}{\leftrightarrow}} [\text{PLC}_z\text{Lp}_n] + [\text{ADP}]$	$k_5 = 1.00,\ k_6 = 10^2$	-	+	-
$[\text{PLC}_z\text{Lp}_n] \underset{8}{\overset{7}{\leftrightarrow}} [\text{ERp57\_Cx/Cr}] + [\text{TAP1/2}] + [\text{Tapasin\_M1}\beta\text{Lp}_n]$	$k_7 = 1.00,\ k_8 = 10^{-6}$	-	+	+
$[\text{Hp}_m] + [\text{ATP\_TAP1/2}] \underset{10}{\overset{9}{\leftrightarrow}} [\text{ATP\_TAP1/2\_Hp}_m]$	$k_9 = 1.00,\ k_{10} = 5.00$	+	+	-
$[\text{Tapasin\_TAP1/2\_M1}\beta\text{\_ERp57\_Cx/Cr}] + [\text{ATP\_TAP1/2\_Hp}_m] \underset{12}{\overset{11}{\leftrightarrow}} [\text{PLC}_z\text{Hp}_m] + [\text{ADP}]$	$k_{11} = 1.00,\ k_{12} = 10^2$	-	+	-
$[\text{PLC}_z\text{Hp}_m] \underset{14}{\overset{13}{\leftrightarrow}} [\text{ERp57\_Cx/Cr}] + [\text{TAP1/2}] + [\text{Tapasin}] + [\text{aM1}\beta]$	$k_{13} = 1.00,\ k_{14} = 10^{-5}$	-	+	+
$[\text{Lp}_n] + [\text{Hp}_m] + [\text{ATP\_TAP1/2}] \underset{16}{\overset{15}{\leftrightarrow}} [\text{ATP\_TAP1/2\_Lp}_n]$	$k_{15} = 1.00,\ k_{16} = 1.00$	+	+	-
$[\text{Tapasin\_M1}\beta\text{Lp}_n] + [\text{Hp}_m] \underset{18}{\overset{17}{\leftrightarrow}} [\text{rM1}\beta] + [\text{Lp}_n] + [\text{Tapasin}]$	$k_{17} = 1.00,\ k_{18} = 32.5$ $k_{18} \in [10^{-6}, 50.0]$	-	+	+
$[\text{Tapasin}] + [\text{ERp57\_Cx/Cr}] \underset{20}{\overset{19}{\leftrightarrow}} [\text{Tapasin\_TAP1/2}]$	$k_{19} = 1.00,\ k_{20} = 10^2$	-	+	-
$[\text{M1}\beta] + [\text{Hp}_m] \underset{22}{\overset{21}{\leftrightarrow}} [\text{M1}\beta\text{Hp}_m]$	$k_{21} = 1.00,\ k_{22} = 0.99$	-	+	-
$[\text{M1}\beta] + [\text{Lp}_n] \underset{24}{\overset{23}{\leftrightarrow}} [\text{M1}\beta\text{Lp}_n]$	$k_{23} = 1.00,\ k_{24} = 0.99$	-	+	-
$[\text{TAP1/2}] + [\text{ATP}] \underset{26}{\overset{25}{\leftrightarrow}} [\text{ATP\_TAP1/2}]$	$k_{25} = 1.00,\ k_{26} = 10^4$	+	+	-
$[\text{rM1}\beta] + [\text{Tapasin}] \underset{28}{\overset{27}{\leftrightarrow}} [\text{Tapasin\_M1}\beta\text{Lp}_n]$	$k_{27} = 1.00,\ k_{28} = 1.01$	-	+	+
$[\text{Lp}_n] + [\text{Hp}_m] + [\text{ATP\_TAP1/2}] \underset{30}{\overset{29}{\leftrightarrow}} [\text{ATP\_TAP1/2\_Hp}_m]$	$k_{29} = 1.00,\ k_{30} = 1.00$	+	+	-

3.2. Theoretical analyses of the LAPD-model of MHC1-mediated high-affinity peptide export

The LAPD-model incorporates several physiologically relevant molecular details of MHC1-mediated export (**Fig. 2**, **Table 2**) [30, 31, 32, 33, 34, 35, 50, 55, 56, 57, 58]. These include: a) the proportion of high- and low-affinity peptides in the cytosol and the ER, b) ATP-driven translocation of ubiquitin-derived cytosolic peptides into the ER lumen through $TAP1/2$, c) assembly of the PLC with Tapasin, ERp57 and $M1\beta$, d) PLC-disassembly and the generation of exportable MHC1 ($eM1\beta$) via the anterograde ($aM1\beta$)- and retrograde/recyclable ($rM1\beta$)-pathways, e) Tapasin-mediated peptide editing of low- with high-affinity variants via the shunt reaction, and f) the contribution of the cis- and trans-faces of the Golgi apparatus ($cGolgi, tGolgi$).

The basic premise of this work is that exportable MHC1 ($eM1\beta$) is not a single entity, but is derived independently from the high- and low-affinity peptide forms of the PLC via the antero ($aM1\beta$)- and retro ($rM1\beta$)-grade pathways (***Eqs.* (16), (17), (18) and (19)**),

$$\begin{aligned} [eM1\beta] &\propto [\boldsymbol{PLC}] \\ &\propto [\boldsymbol{PLCHp + PLCLp}] \\ [eM1\beta(t)] &= \gamma.\int_{z=1}^{z=N} \left(\left[PLC_zHp_m(t)\right] + \left[PLC_zLp_n(t)\right] \right) \\ &= \gamma.\left(\int_{z=1}^{z=N} \left[PLC_zHp_m(t)\right] + \int_{z=1}^{z=N} \left[PLC_zLp_n(t)\right] \right) \end{aligned} \tag{20}$$

Case (1): Consider an arbitrary high-affinity peptide in complex with the MHC1-complex $\left(M1\beta Hp_m\right)$. This interaction will abrogate the interaction between MHC1 and Tapasin $\left(PLC_zHp_m \sim PPI_{Erp57-Tapasin} + M1\beta Hp_m\right)$ prior to autocatalytic reduction [53]. This results in the appearance of anterograde-derived $M1\beta$ and readily exportable ($aM1\beta$) in the ER lumen and thence at the plasma membrane ($eM1\beta$) (**Fig. 2**) [59, 60, 61]. This can be represented as:

$$PLC_zHp_m \rightarrow TAP1/2 + ERp57 + Tapasin + M1\beta Hp_m$$
$$M1\beta Hp_m \equiv aM1\beta \xrightarrow{cGolgi \rightarrow tGolgi} eM1\beta$$

Combining the aforementioned partial reactions and incorporating the observation that $TAP1/2$ is membrane bound we can rewrite this,

$$PLC_zHp_m \rightarrow ERp57 + Tapasin + aM1\beta$$

As indicated previously MHC1-mediated export of high-affinity peptides is characterized by protein-protein interactions and inter-molecular complex formation. Rewriting the left hand side of the above reaction as molar concentrations of the component complexes of PLC,

$$\left[PLC_zHp_m\right] = \left[PPI_{ERp57-Tapasin}\right].\left[PPI_{Tapasin-M1\beta Hp_m}\right] \tag{20.1}$$

Using these we can derive a numerical expression for the high-affinity peptide bound form of the PLC $\left(PLC_zHp_m\right)$,

$$(\textbf{Abrogation, dissassociation}) = \left[PPI_{ERp57-Tapasin}\right].\left[M1\beta Hp_m\right] \tag{20.2}$$

$$(\textbf{Autocatlytic reduction}) = [ERp57].[Tapasin].[aM1\beta] \tag{20.3}$$

***Combining equations* (20.2) *and* (20.3)**

$$\left[PLC_zHp_m\right] = [ERp57].[Tapasin].[aM1\beta] \tag{20.4}$$

***Solving equation* (20.4)**

$$Log\left[PLC_zHp_m\right] = Log([ERp57].[Tapasin].[aM1\beta]) \tag{20.5}$$

$$= Log[ERp57] + Log[Tapasin] + Log[aM1\beta] \tag{20.6}$$

$$\frac{d\left(Log\left[PLC_zHp_m\right]\right)}{d\left[PLC_zHp_m\right]} = (Log[ERp57] + Log[Tapasin] + Log[aM1\beta]) \tag{20.7}$$

$$d\left(Log\left[PLC_zHp_m\right]\right) = (Log[ERp57] + Log[Tapasin] + Log[aM1\beta])\,d\left[PLC_zHp_m\right]$$
$$\int d\left(Log\left[PLC_zHp_m\right]\right) = \int (Log[ERp57] + Log[Tapasin] + Log[aM1\beta])\,d\left[PLC_zHp_m\right] \tag{20.8}$$

$$\frac{1}{\left[PLC_zHp_m\right]} = \left(\int Log[ERp57] + \int Log[Tapasin] + \int Log[aM1\beta]\right) d\left[PLC_zHp_m\right]$$
$$= \frac{1}{2}.([ERp57] + [Tapasin] + [aM1\beta]) + \frac{c}{2} \tag{20.9}$$

***Rearranging equation* (20.9)**

$$\left[PLC_zHp_m\right] = \frac{2}{([ERp57] + [Tapasin] + [aM1\beta])} + \frac{2}{c}$$
$$= \frac{2}{([ERp57] + [Tapasin] + [aM1\beta])} + c_{[PLC_zHp_m]} \tag{21}$$

Here, c and $c_{[PLC_zHp_m]}$ represent arbitrary constants of the solutions of the equations to establish the molar concentration of PLC_zHp_m.

Case (2): The presence of a low-affinity peptide in complex with the MHC1-complex $\left(M1\beta Lp_n\right)$ leads to the persistence of the corresponding PLC $\left(PLC_zLp_n\right)$. The autocatalytic reduction or "reductive escape" of the ternary complex of bound Tapasin with $M1\beta$ ($PLC_zLp_n \sim PPI_{Tapasin-M1\beta Lp_n} + ERp57$) is then the *de facto* primary reaction [53]. This results in the appearance of the Tapasin-driven recyclable $M1\beta$ at COPI-exit sites of the ER [62].

$$PLC_zLp_n \rightarrow TAP1/2 + ERp57 + PPI_{Tapasin-M1\beta Lp_n}$$
$$PPI_{Tapasin-M1\beta Lp_n} \xrightarrow{ER \leftrightarrow cGolgi} PPI_{Tapasin-M1\beta Lp_n}$$

We can exclude $TAP1/2$ (membrane bound) and rewrite the combined reaction as,

$$PLC_zLp_n \rightarrow ERp57 + PPI_{Tapasin-M1\beta Lp_n}$$

Rewriting the left hand side as molar concentrations of the component complexes of PLC,

$$\left[PLC_zLp_n\right] = [ERp57].\left[PPI_{Tapasin-M1\beta Lp_n}\right] \tag{21.1}$$

In the presence of a random high-affinity peptide anywhere else along the pathway, the "shunt"-reaction is triggered. The ternary complex of Tapasin then rapidly disassociates to yield exportable $M1\beta$.

$$PPI_{Tapasin-M1\beta Lp_n} \xrightarrow{Hp_m} Tapasin + Lp_n + M1\beta Hp_m$$
$$M1\beta Hp_m \equiv rM1\beta \xrightarrow{cGolgi \rightarrow tGolgi} eM1\beta$$

Rewriting the left hand side of "shunt"-reaction along with the generated exportable $M1\beta$ $\left(M1\beta Hp_m \equiv rM1\beta\right)$,

$$\left[PPI_{Tapasin-M1\beta Lp_n}\right] = [Tapasin].\left[Lp_n\right].\left[M1\beta Hp_m\right] \tag{21.2}$$

$$= [Tapasin].\left[Lp_n\right].[rM1\beta] \tag{21.3}$$

***Combining equations* (21.1) *and* (21.3)**

$$\left[PLC_zLp_n\right] = [ERp57].[Tapasin].\left[Lp_n\right].[rM1\beta] \tag{21.4}$$

***Solving equation* (21.4)**

$$Log\left[PLC_zLp_n\right] = Log\left(\left[ERp57\right].\left[Tapasin\right].\left[Lp_n\right].\left[rM1\beta\right]\right) \tag{21.5}$$

$$= Log\left[ERp57\right] + Log\left[Tapasin\right] + Log\left[Lp_n\right] + Log\left[rM1\beta\right] \tag{21.6}$$

$$\frac{d\left(Log\left[PLC_zLp_n\right]\right)}{d\left[PLC_zLp_n\right]} = \left(Log\left[ERp57\right] + Log\left[Tapasin\right] + Log\left[Lp_n\right] + Log\left[rM1\beta\right]\right) \tag{21.7}$$

$$d\left(Log\left[PLC_zLp_n\right]\right) = \left(Log\left[ERp57\right] + Log\left[Tapasin\right] + Log\left[Lp_n\right] + Log\left[rM1\beta\right]\right) d\left[PLC_zLp_n\right]$$

$$\int d\left(Log\left[PLC_zLp_n\right]\right) = \int \left(Log\left[ERp57\right] + Log\left[Tapasin\right] + Log\left[Lp_n\right] + Log\left[rM1\beta\right]\right) d\left[PLC_zLp_n\right] \tag{21.8}$$

$$\frac{1}{\left[PLC_zLp_n\right]} = \left(\int Log\left[ERp57\right] + \int Log\left[Tapasin\right] + \int Log\left[Lp_n\right] + \int Log\left[rM1\beta\right]\right) d\left[PLC_zLp_n\right]$$

$$= \frac{1}{2}.\left(\left[ERp57\right] + \left[Tapasin\right] + \left[Lp_n\right] + \left[rM1\beta\right]\right) + \frac{c}{2} \tag{21.9}$$

***Rearranging equation* (21.9)**

$$\left[PLC_zLp_n\right] = \frac{2}{\left(\left[ERp57\right] + \left[Tapasin\right] + \left[Lp_n\right] + \left[rM1\beta\right]\right)} + \frac{2}{c}$$

$$= \frac{2}{\left(\left[ERp57\right] + \left[Tapasin\right] + \left[Lp_n\right] + \left[rM1\beta\right]\right)} + c_{\left[PLC_zLp_n\right]} \tag{22}$$

Here, c and $c_{\left[PLC_zLp_n\right]}$ represent arbitrary constants of the solutions of the equations to establish the molar concentration of PLC_zLp_n.

Substituting equations (21) and (22) in equation (20),

$$\left[eM1\beta\right] = \frac{2.\left(2.\left[ERp57\right] + 2.\left[Tapasin\right] + \left[Lp_n\right] + \left[aM1\beta\right] + \left[rM1\beta\right]\right)}{\left(\left[ERp57\right] + \left[Tapasin\right] + \left[aM1\beta\right]\right).\left(\left[ERp57\right] + \left[Tapasin\right] + \left[Lp_n\right] + \left[rM1\beta\right]\right)} + c_{\left[eM1\beta\right]} \tag{23}$$

where $c_{\left[eM1\beta\right]}$ is the combined arbitrary constant of the solution of the equation to establish the molar concentration of exportable MHC1,

$$c_{\left[eM1\beta\right]} = c_{\left[PLC_zHp_m\right]} + c_{\left[PLC_zLp_n\right]} \tag{23.1}$$

It is clear from Equation (23) that the final exportable form of MHC1 ($eM1\beta$) is complex and dependent on the concentrations of unbound low-affinity peptides, Tapasin, ERp57, antero ($aM1\beta$)- and retro ($rM1\beta$)-grade derived fractions of MHC1.

3.3. Elucidating the molecular biology of the LAPD-model of MHC1-mediated high-affinity peptide export

Comprehending the underlying molecular mechanism(s) that constitute MHC1-mediated high-affinity peptide export mandates formulating and simulating the CME of net exportable MHC1. The resulting data can then be used to numerically approximate the CME and infer biological function.

3.3.1. Formulating the CME of net exportable MHC1

Equation (23), suggests that exportable or high-affinity peptide bound MHC1 ($eM1\beta$) is generated concomitantly by the antero ($aM1\beta$)- and retro ($rM1\beta$)-grade pathways ($eM1\beta = aM1\beta + rM1\beta$). However, the origin and temporal variation of these proportions is unclear. Although multifactorial, peptide editing and the production of $rM1\beta$, along with *de novo* $aM1\beta$-generation are probably major contributors. In order to gain insights into these phenomena a time-dependent mathematical expression of exportable MHC1, i.e., the CME of net exportable MHC1 ($|\Delta\left[eM1\beta\right](t)|$) is formulated.

Using $\left\{\left[Hp_m(t=0)\right], \left[Lp_n(t\gg 0)\right]\right\} \to 0$ and equations (16) and (17) to rewrite equation (23),

$$\left[eM1\beta(t\to 0)\right] = \frac{2.\left(2.\left[ERp57\right] + 2.\left[Tapasin\right] + \left[Lp_n\right] + \left[rM1\beta\right]\right)}{\left(\left[ERp57\right] + \left[Tapasin\right]\right)\left(\left[ERp57\right] + \left[Tapasin\right] + \left[Lp_n\right] + \left[rM1\beta\right]\right)} \tag{24}$$

$$\left[eM1\beta(t\gg 0)\right] = \frac{2.\left(2.\left[ERp57\right] + 2.\left[Tapasin\right] + \left[aM1\beta\right]\right)}{\left(\left[ERp57\right] + \left[Tapasin\right]\right)\left(\left[ERp57\right] + \left[Tapasin\right] + \left[aM1\beta\right]\right)} \tag{25}$$

Simplifying equations (24) and (25) as partial fractions,

$$\left[eM1\beta(t\to 0)\right] = \frac{2}{\left(\left[ERp57\right] + \left[Tapasin\right]\right)} + \frac{2}{\left(\left[ERp57\right] + \left[Tapasin\right] + \left[Lp_n\right] + \left[rM1\beta\right]\right)} \tag{26}$$

$$\left[eM1\beta(t\gg 0)\right] = \frac{2}{\left(\left[ERp57\right] + \left[Tapasin\right]\right)} + \frac{2}{\left(\left[ERp57\right] + \left[Tapasin\right] + \left[aM1\beta\right]\right)} \tag{27}$$

Rearranging and equating,

$$\left|\left[eM1\beta(t\to 0)\right] - \left[eM1\beta(t\gg 0)\right]\right| = \left|-\gamma.\left(\left(\left[Lp_n(t)\right] + \left[rM1\beta(t)\right]\right) - \left[aM1\beta(t)\right]\right)\right| \tag{28}$$

where,

$$\gamma = \frac{2}{\left(\left[ERp57(t)\right] + \left[Tapasin(t)\right] + \left[Lp_n(t)\right] + \left[rM1\beta(t)\right]\right)\left(\left[ERp57(t)\right] + \left[Tapasin(t)\right] + \left[aM1\beta(t)\right]\right)} \tag{28.1}$$

Rewriting equation (28)

$$\left|\Delta\left[eM1\beta\right](t)\right| = \left|-\gamma.\left(\left(\left[Lp_n(t)\right] + \left[rM1\beta(t)\right]\right) - \left[aM1\beta(t)\right]\right)\right| \tag{29}$$

Clearly, the time-dependent CME of exportable MHC1 is influenced by the proportion of antero ($aM1\beta$)- and retro ($rM1\beta$)-grade derived fractions of MHC1. Equation (29), also highlights the non-trivial role that low-affinity peptides may have in the genesis of exportable MHC1. These analyses suggest that the LAPD-model may be the dominant operative mechanism *in vivo*, by which MHC1 exports high-affinity peptides to the plasma membrane of nucleated cells.

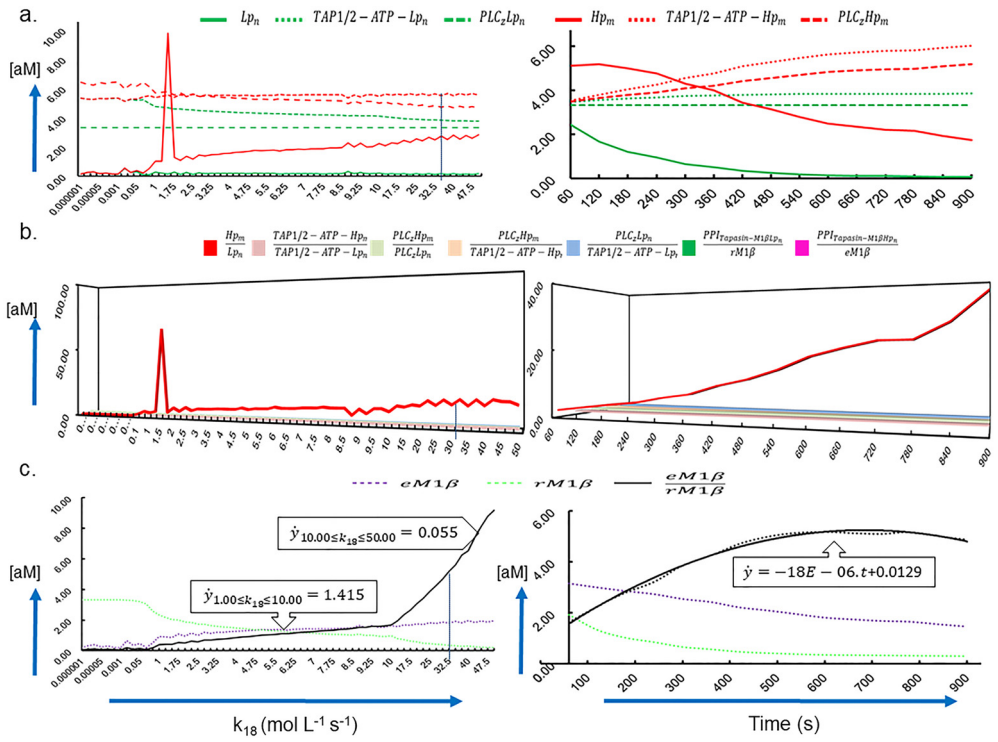

Fig. 3. Insights into the molecular biology of the LAPD-model of MHC1-mediated export. a), b) High- ($Hp_m \in \boldsymbol{Hp}$) and low- ($Lp_n \in \boldsymbol{Lp}$) affinity peptides are translocated across the ER membrane and result in differential forms of the PLC, i.e., $\{PLC_z \in \boldsymbol{PLC} | PLC_z \sim PLC_z - Lp_n \vee PLC_z - Hp_m\}$, and other intermediate complexes ($PPI_{ERp57-Tapasin}$, $PPI_{Tapasin-M1\beta Lp_n}$). An important result is that while the concentration of unbound low-affinity peptides progressively declines, high-affinity peptides accumulate in the ER lumen. This progressive enrichment, is all the more relevant since low-affinity peptides are almost five orders of magnitude in excess at any given time. Additionally, this implies a temporal bisection of the MHC1-mediated export of high-affinity peptides into "early"- and "late"-phases, and c) Simulation studies of the LAPD-model of exportable MHC1. The CME of net exportable MHC1 ($eM1\beta(t)$), is a complex mathematical expression that involves interactions between Tapasin, ERp57, low- and high-affinity peptides, TAP1/2, and $M1\beta$. A key finding of the early-phase is that the shunt reaction ($PPI_{Tapasin-M1\beta-Lp_n} + Hp_m \rightarrow Tapasin + Lp_n + rM1\beta$) ($RXN$ 18) is rate limiting. The LAPD-model is parameterized ($k_{18} = 30 - 35$ mol L^{-1} s^{-1}) on the basis of empirical data ($\frac{[eM1\beta]}{[rM1\beta]} \approx 5.00$). **Abbreviations: $\boldsymbol{aM1\beta}$**, anterograde-derived fraction of exportable MHC1; **ER**, endoplasmic reticulum; **$\boldsymbol{k_{18}}$**, rate constant for reaction 18; **$\boldsymbol{M1\beta}$**, major histocompatibility I antigen in complex with β_2-microglobulin; **$\boldsymbol{eM1\beta}$**, exportable MHC1; **MHC1**, major histocompatibility complex I antigens; **PLC**, set of differential forms of the peptide loading complex; **PPI**, protein-protein interaction; **$\boldsymbol{rM1\beta}$**, retrograde-derived fraction of exportable MHC1; **$\boldsymbol{RXN}$**, reaction.

3.3.2. The LAPD-model suggests that the recyclable fraction of MHC1 is a significant early contributor to exportable MHC1

Although PLC assembly/disassembly is bimodal, the theoretical results and simulation data from this study suggests that the contribution of the anterograde- and retrograde-pathways to exportable MHC1 is also distinctly biphasic (early, late). A key finding of the "early"-phase is that the shunt reaction ***Eqs.* (21.2), (21.3)** (RXN 18) is rate limiting. This data ($k_{18} \in [10^{-6}, 50], n = 65$) is robust for $k_{18} \geq 10.00$ mol L^{-1} s^{-1} and can be parameterized ($k_{18} = 30 - 35$ mol L^{-1} s^{-1}) (**Fig. 3**; **Supplementary Table 3**). This choice is based on the empirical observation ($\frac{[eM1\beta]}{[rM1\beta]} \approx 5.00$) and is corroborated directly by comparing the proportion of net exportable-MHC1 generated by the retrograde pathway ($1.64 \leq \frac{[eM1\beta(t)]}{[rM1\beta(t)]} \leq 4.87$) ***Eqs.* (36), (37), (38), (39) and (40) (Fig. 3, Table 3)**. Thus, while the retrograde/recyclable fraction is an "early"-contributor, the anterograde-derived fraction of exportable MHC1 contributes to the MHC1-mediated export of high-affinity peptides at "later" time points.

3.3.3. The LAPD-model of exportable MHC1 leads to enrichment of high-affinity peptides in the ER lumen

Cytosolic-derived peptides ($\boldsymbol{Hp} \cup \boldsymbol{Lp}$) are translocated across the ER membrane in association with $TAP1/2$ in an ATP-dependent step. Interestingly, and in complete contrast to their baseline levels, the concentrations of the unbound peptides exhibit an exponential increase ***Eq.* (52)** (**Figs. 3a and 3b, Table 4**). These findings are intriguing given that the initial concentrations of the PLC ($y_{[PLC_zHp_m(t_0)]} \cong y_{[PLC_zLp_n(t_0)]}$) are equivalent and the contribution of the intermediate complexes is trivial ***Eqs.* (53), (54)** (**Figs. 3a and 3b, Table 4**). Additional findings include the relatively unchanging concentration of the low-affinity peptide bound form of the PLC and the progressive enrichment in the ER-lumen of the high-affinity peptide bound variant ***Eqs.* (55), (56)** (**Figs. 3a and 3b, Table 4**).

4. Discussion

The release of MHC1 from the PLC is a critical event in the export and presentation of endogenously derived intracellular peptides to the surface of nucleated cells. Since this occurs preferentially for high-affinity peptides, insights into the molecular mechanisms that regulate these steps may be relevant to disease progression.

4.1. Low-affinity peptides can regulate MHC1-mediated export of high-affinity peptides

The LAPD-model bisects MHC1-mediated export of high-affinity peptides into an "early"- ($t \leq 600$ s) and "late"- ($t > 600$ s) phase. The "early"-phase is characterized by the kinetics of disassembly and exchange, and is mediated by the shunt reaction (**Figs. 3c and 4a**). In fact, simulation data

Table 3. Regression equations and assessment of robustness of time-dependent behavior of molecular entities in the LAPD-model of MHC1-mediated export of high-affinity peptides.

Molecule (s) $\{y_k, y, y1\,(x, y)\}$	$\{y_k = f(k), y = f(t), y1 = f(t)\}$	R^2	Equation
High − affinity peptide	$y = 6.2158.e^{-0.085.t}$	0.9818	(30)
Low − affinity peptide	$y = 2.6422E - 0.273.t$	0.9839	(31)
$PPI_{TAP1/2-ATP-Hp_m}$	$y = 1.0389.\ln(t) + 3.1197$	0.9518	(32)
$PPI_{TAP1/2-ATP-Lp_n}$	$y = 0.1511.\ln(t) + 3.4803$	0.9751	(33)
PLC_zLp_n	$y = 3.32$	1.0000	(34)
PLC_zHp_m	$y = 0.1234.t + 3.4652$	0.9743	(35)
$rM1\beta$	$y = -0.582.\ln(t) + 4.1018$	0.9498	(36)
$PPI_{Tapasin-M1\beta Lp_n}$	$y = 0.5842.\ln(t) + 4.9181$	0.9507	(37)
$eM1\beta$	$y = 3.338.e^{-0.057.t}$	0.9916	(38)
$\frac{eM1\beta}{rM1\beta}$	$y_k = \begin{cases} 0.1415.k + 0.2718, & k_{18} \in [1.00, 10.00] \\ 1.2764.e^{0.0415.k}, & k_{18} \in [10.00, 50.00] \end{cases}$	0.9961 0.9868	(39)
$\frac{eM1\beta}{rM1\beta}$	$y = -9E - 06.t^2 + 0.0129.t + 0.8294$	0.9943	(40)
$aM1\beta$	$y = 0.0019.t^3 - 0.0536.t^2 + 0.3998.t + 0.9851$	0.9459	(41)
Tapasin	$y = -1.273.\ln(t) + 6.8514$	0.9945	(42)
ERp57	$y = -0.1234.t + 4.0051$	0.9748	(43)
ERp57 and Tapasin	$y1 = 1.428.e^{0.372.t}$	0.9854	(44)
$PPI_{Tapasin-M1\beta Lp_n}$ and Tapasin	$y1 = -0.9949.t^2 + 9.142.t - 14.336$	0.9855	(45)
$eM1\beta$ and Low − affinity peptides	$y1 = 0.8978.x^3 - 5.0364.x^2 + 9.6748.x - 6.1758$	0.9972	(46)
$eM1\beta$ and $rM1\beta$	$y1 = 0.7206.x^3 - 4.1556x^2 + 8.1046.x - 4.9555$	0.9947	(47)
$eM1\beta$ and $aM1\beta$	$y1 = -0.7219.x^3 + 4.15x^2 - 7.0732.x + 4.9153$	0.9819	(48)
$eM1\beta$ and Tapasin	$y1 = 0.735.x^3 - 4.2607.x^2 + 9.3535.x - 3.4876$	0.9988	(49)
$eM1\beta$ and ERp57	$y1 = x + 0.83$	1.0000	(50)
$eM1\beta$ and ATP	$y1 = -0.0105.x^3 + 0.4871.x^2 - 1.366.x + 3.7575$	0.9997	(51)

Table 4. Temporal profile of molecular entities in the LAPD-model of MHC1-mediated export of high-affinity peptides.

Equation/Expression/Equivalence	No.	Molecular entity $\{y, y1\}$
$1 \leq \frac{\dot{y}_{[Hp_m(t_0)]}}{\dot{y}_{[Lp_n(t_0)]}} \ll \frac{\dot{y}_{[Hp_m(t)]}}{\dot{y}_{[Lp_n(t)]}}$	(52)	Equations (30), (31)
$\dot{y}\left[PPI_{TAP1/2-ATP-Hp_m}\right] \to 0$	(53)	Equation (32)
$\dot{y}\left[PPI_{TAP1/2-ATP-Lp_n}\right] \to 0$	(54)	Equation (33)
$\dot{y}_{[PLC_zLp_n(t)]} = 0$	(55)	Equation (34)
$\dot{y}_{[PLC_zHp_m(t)]} \approx 0.1234$	(56)	Equation (35)
$0.35 \leq \frac{\dot{y}_{[rM1\beta(t)]}}{\dot{y}_{\left[PPI_{Tapasin-M1\beta Lp_n}(t)\right]}} \leq 0.5$	(57)	Equations (36), (37)
$\dot{y}_{[rM1\beta(t)]} \simeq \frac{0.582}{t} \to 0\ (t \gg 0)$	(58)	Equation (36)
$\dot{y}_{[eM1\beta(t)]} \sim 3 * 0.0003 * t^2 - 2 * 0.0034 * t - 0.145$	(59)	Equation (38)
$\dot{y}\left[PPI_{Tapasin-M1\beta Lp_n}(t)\right] \simeq \frac{0.5842}{t} \to 0\ (t \gg 0)$	(60)	Equation (37)
$\dot{y}_{[Lp_n(t)]} \to 0\ (t \gg 0)$	(61)	Equation (31)
$\dot{y}_{[Tapasin(t)]} \simeq \frac{-1.273}{t} \to 0\ (t \gg 0)$	(62)	Equation (42)
$\dot{y}1_{[ERp57(t)],[Tapasin(t)]} \to 1.00$	(63)	Equations (42), (43) and (44)
$\dot{y}_{[PPI_{Tapasin-M1\beta Lp_n}(t)]} \propto \frac{1}{\dot{y}_{[Tapasin(t)]}}$	(64)	Equations (37), (42)
$\dot{y}_{[PLC_zHp_m(t)]} \propto \frac{1}{\dot{y}_{[Tapasin(t)]}}$	(65)	Equations (35), (42)

suggests that more than 50% of $PPI_{Tapasin-M1\beta Lp_n}$ that exits the ER via the retrograde pathway is potentially exchangeable with the high-affinity variant ($rM1\beta \approx 61\%, aM1\beta \approx 39\%$) ***Eq.* (57)** (**Table 4**). Interestingly, the data also suggests that the contribution by the retrograde pathway to the exportable MHC1 is self-limiting and will progressively diminish ***Eqs.* (58), (59)** (**Figs. 3c and 4a, Table 4**). This implies that the "shunt"-reaction mediated peptide editing that results from this exchangeable fraction is saturable ***Eq.* (60)** (**Fig. 4a and 4c, Table 4**). This is in part due to unbound Tapasin and low-affinity peptides being progressively depleted ***Eqs.* (61), (62)** (**Figs. 4a and 4c, Table 4**). Prior to the complete exhaustion of low-affinity peptides, equivalent quantities of unbound Tapasin, ERp57 $\left(PLC_zLp_n \rightleftarrows PPI_{Tapasin-M1\beta Lp_n} \rightleftarrows \{Tapasin, ERp57\}\right)$ and a progressively increasing concentration of untransported high-affinity peptides participates in the *de novo* assembly of PLC_zHp_m (**Figs. 4b and 4c**). The ensuing "late"-phase is then characterized by rapid disassociation of the PLC, linear increase in the concentration of PLC_zHp_m and the equivalent pairing of Tapasin and ERp57. Anterograde-derived MHC1, is therefore, a significant contributor to MHC1-mediated peptide export ($rM1\beta \approx 21\%$, $aM1\beta \approx 79\%$) at later time points ***Eqs.* (56), (63)** (**Figs. 4b and 4c, Table 4**).

4.2. Elucidating the role of Tapasin in MHC1-mediated high-affinity peptide export

Tapasin is a critical modulator in the MHC1-mediated export of high-affinity peptides. Since, Tapasin is absent from the final exportable MHC1 its role is indirect, i.e., of a facilitator and regulator [67]. However, the molecular mechanism(s) by which Tapasin accomplishes this is unclear. The LAPD-model suggests that the proportion of unbound- and bound $\left(PPI_{ERp57-Tapasin}, PPI_{Tapasin-M1\beta Lp_n}\right)$-Tapasin may influence MHC1-mediated high-affinity peptide export. Simulation data suggests that the concentration of unbound Tapasin varies inversely with $PPI_{Tapasin-M1\beta Lp_n}$, is non-linear and skewed ***Eq.* (64)** (**Fig. 4a, Table 4**). This implies that Tapasin can partake in the *de novo* assembly and subsequent disassembly of the PLC in the presence of high-affinity peptides ***Eq.* (65)** (**Fig. 4b, Table 4**). The LAPD-model also lends support to the molecular plasticity of Tapasin and suggests a role in the "early"- and "late"-phases of MHC1-mediated export of high-affinity peptides to the plasma membrane. The presence of

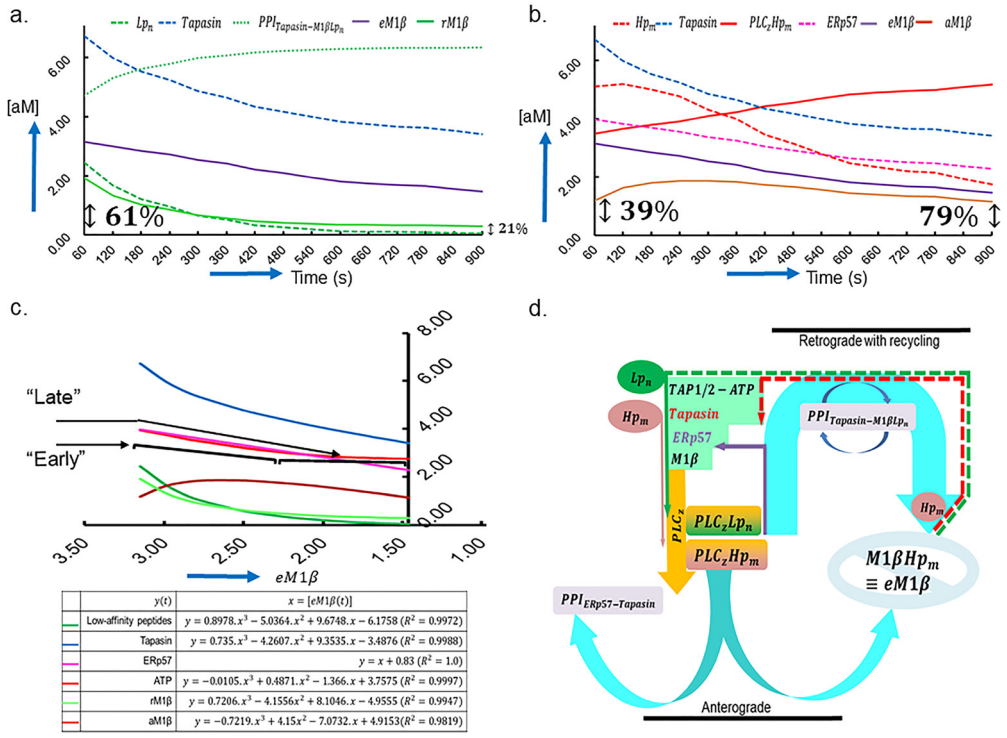

	$y(t)$	$x = [eM1\beta(t)]$
	Low-affinity peptides	$y = 0.8978.x^3 - 5.0364.x^2 + 9.6748.x - 6.1758$ ($R^2 = 0.9972$)
	Tapasin	$y = 0.735.x^3 - 4.2607.x^2 + 9.3535.x - 3.4876$ ($R^2 = 0.9988$)
	ERp57	$y = x + 0.83$ ($R^2 = 1.0$)
	ATP	$y = -0.0105.x^3 + 0.4871.x^2 - 1.366.x + 3.7575$ ($R^2 = 0.9997$)
	rM1β	$y = 0.7206.x^3 - 4.1556x^2 + 8.1046.x - 4.9555$ ($R^2 = 0.9947$)
	aM1β	$y = -0.7219.x^3 + 4.15x^2 - 7.0732.x + 4.9153$($R^2 = 0.9819$)

Fig. 4. Low-affinity peptides can bisect and thereby regulate MHC1-mediated export. a) The "early"-phase is self-limiting, saturable and dependent on the concentration of $PPI_{Tapasin-M1\beta Lp_n}$. Here, the generation of exportable MHC1 predominantly occurs by competitive binding and thence exchange of bound low-affinity peptides with high-affinity variants. The ensuing cycles of peptide editing ensures progressive enrichment of high-affinity peptides in the ER lumen along with equivalent quantities of unbound Tapasin and ERp57, b) the "late"-phase of MHC1-mediated export of high-affinity peptides is facilitated by the near exhaustion of low-affinity peptides and the *de novo* assembly of PLC bound with high-affinity peptides. The continued sequestration of Tapasin and ERp57 leads to declining levels of these. The rapid disassembly implies that exportable MHC1 generated by the anterograde pathway is a significant contributor to the export of high-affinity peptides, c) and d) physiological relevance and biochemical basis of LAPD-model of MHC1-mediated high-affinity peptide export. The LAPD-model bisects MHC1-mediated export of high-affinity peptides to the plasma membrane and is able to offer plausible explanations into empirically observed phenomena. The theoretical analyses and simulation data presented also demonstrate mechanism(s) by which altered cells may "flag" circulating T- and B-cells and thence present intracellular peptide immunogens rapidly and sustainably. **Abbreviations: ER**, endoplasmic reticulum; **Hp,** set of high-affinity peptides; **Lp,** set of low-affinity peptides; $eM1\beta$, exportable MHC1; **MHC1**, major histocompatibility I antigen; **PLC**, set of differential forms of the peptide loading complex; **PPI**, protein-protein interaction; **ATP**, adenosine triphosphate; $M1\beta$, heterodimer of major histocompatibility I antigen in complex with β_2-microglobulin.

a transmembrane-domain and the propensity to form extensive protein-protein interaction surfaces concomitantly with TAP1/2, ERp57, and MHC1 suggest that the role of Tapasin as a master regulator may be justified [38, 39, 40, 41, 46, 47, 48, 49, 50].

4.3. LAPD-model of MHC1-mediated high-affinity peptide export may offer insights into adaptive immunosurveillance

Intracellular immunogens that result from cytoplasmic infections and dysplastic cellular alterations of a host cell can elicit a spectrum of responses from circulating T- and B-cells. These include tolerance, apoptosis and autoimmune-mediated lysis of the affected cell. The LAPD-model posits that a critical mass of exchangeable MHC1 ($rM1\beta \approx 61\%$) is necessary to execute immediate export and present a novel peptide-immunogen to circulating T- and B-cells **(Figs. 4a, 4c and 4d)**. The *de novo* PLC-assembly/disassembly that occurs subsequently will, in turn, generate sufficient exportable MHC1 ($aM1\beta \approx 79\%$) for a sustained immune response **(Figs. 4b, 4c and 4d)**. The LAPD-model also offers plausible explanations into the empirically observed negative regulation by soluble Tapasin on MHC1-mediated export of high-affinity peptides [68]. In particular, soluble Tapasin might result in the complete abrogation of the "early"-phase, *viz.* peptide editing and the retrograde-derived exportable $M1\beta$ **(Figs. 4c and 4d)**. Furthermore, since unbound Tapasin is also a pre-requisite for the "late"-phase, molecular mechanism(s) which sequester Tapasin may severely dampen the magnitude of this phase as well **(Figs. 4c and 4d)**. The findings presented, whilst, re-affirming the significance of Tapasin, also emphasizes the regulatory influence of low-affinity peptides, ERp57 and ATP **(Figs. 4c and 4d)**. For example, dysplastic cellular development can saturate the ATP-driven translocation mechanism with low affinity peptides [36, 37, 38]. This will not only deplete ATP, but also ensure that Tapasin is perpetually in complex with $M1\beta$ **(Figs. 4c and 4d)**. Consequently, even if the proportion of high-affinity peptides was high the absence of ATP would render MHC1-mediated peptide export ineffective and unviable. A similar analogy might operate for ERp57 wherein, the absence/paucity of the mature protein may retard PLC-assembly/disassembly kinetics [46, 54]. Similarly, ATP-depletion is utilized by the human cytomegalovirus glycoprotein US6 to inhibit peptide translocation across the ER [6, 69, 70].

5. Conclusions

The adaptive immune response mandates that potential immunogens are presented in adequate quantities and in a sustained manner to circulating T- and B-cells. MHC1-based export of endogenous intracellular peptides is a complex interplay of molecules (high- and low-affinity peptides, TAP1/2, Tapasin, ERp57, ATP) and higher-order complexes. The LAPD-model, bisects MHC1-mediated export of high-affinity peptides into distinct

time-dependent “early”- and “late”-phases. The total exportable MHC1 is initially dominated by the retrograde (recyclable)- and later by the anterograde (*de novo*)-pathway. Future models will explore cross-presentation of endo- and exo-genous proteins by MHC1 and MHC2, non-protein immunogen presentation, as well as perturbed antigen presentation in the pathogenesis of autoimmune diseases.

Declarations

Author contribution statement

Siddhartha Kundu: Conceived and designed the experiments; Performed the experiments; Analyzed and interpreted the data; Contributed reagents, materials, analysis tools or data; Wrote the paper.

Funding statement

This research did not receive any specific grant from funding agencies in the public, commercial, or not-for-profit sectors.

Data availability statement

Data included in article/supplementary material/referenced in article.

Declaration of interests statement

The authors declare no conflict of interest.

Additional information

Supplementary content related to this article has been published online at https://doi.org/10.1016/j.heliyon.2021.e07466.

References

[1] A. Castro-Prieto, B. Wachter, S. Sommer, Cheetah paradigm revisited: MHC diversity in the world’s largest free-ranging population, Mol. Biol. Evol. 28 (2011) 1455–1468.
[2] H.V. Siddle, C. Sanderson, K. Belov, Characterization of major histocompatibility complex class I and class II genes from the Tasmanian devil (Sarcophilus harrisii), Immunogenetics 59 (2007) 753–760.
[3] L. Zhu, X.D. Ruan, Y.F. Ge, Q.H. Wan, S.G. Fang, Low major histocompatibility complex class II DQA diversity in the Giant Panda (Ailuropoda melanoleuca), BMC Genet. 8 (2007) 29.
[4] K. Belov, J.E. Deakin, A.T. Papenfuss, M.L. Baker, S.D. Melman, H.V. Siddle, N. Gouin, D.L. Goode, T.J. Sargeant, M.D. Robinson, M.J. Wakefield, S. Mahony, J.G. Cross, P.V. Benos, P.B. Samollow, T.P. Speed, J.A. Graves, R.D. Miller, Reconstructing an ancestral mammalian immune supercomplex from a marsupial major histocompatibility complex, PLoS Biol. 4 (2006) e46.
[5] W. Babik, W. Durka, J. Radwan, Sequence diversity of the MHC DRB gene in the Eurasian beaver (Castor fiber), Mol. Ecol. 14 (2005) 4249–4257.
[6] E.W. Hewitt, The MHC class I antigen presentation pathway: strategies for viral immune evasion, Immunology 110 (2003) 163–169.
[7] J.K. Kulski, T. Shiina, T. Anzai, S. Kohara, H. Inoko, Comparative genomic analysis of the MHC: the evolution of class I duplication blocks, diversity and complexity from shark to man, Immunol. Rev. 190 (2002) 95–122.
[8] The MHC sequencing consortium, Complete sequence and gene map of a human major histocompatibility complex. The MHC sequencing consortium, Nature 401 (1999) 921–923.
[9] K. Yamazaki, E.A. Boyse, V. Mike, H.T. Thaler, B.J. Mathieson, J. Abbott, J. Boyse, Z.A. Zayas, L. Thomas, Control of mating preferences in mice by genes in the major histocompatibility complex, J. Exp. Med. 144 (1976) 1324–1335.
[10] C. Linscheid, M.G. Petroff, Minor histocompatibility antigens and the maternal immune response to the fetus during pregnancy, Am. J. Reprod. Immunol. 69 (2013) 304–314.
[11] M. Dzierzak-Mietla, M. Markiewicz, U. Siekiera, S. Mizia, A. Koclega, P. Zielinska, M. Sobczyk-Kruszelnicka, S. Kyrcz-Krzemien, Occurrence and impact of minor histocompatibility antigens’ disparities on outcomes of hematopoietic stem cell transplantation from HLA-matched sibling donors, Bone Marrow Res. 2012 (2012) 257086.
[12] N.J. Robertson, J.G. Chai, M. Millrain, D. Scott, F. Hashim, E. Manktelow, F. Lemonnier, E. Simpson, J. Dyson, Natural regulation of immunity to minor histocompatibility antigens, J. Immunol. 178 (2007) 3558–3565.
[13] C. Perreault, F. Decary, S. Brochu, M. Gyger, R. Belanger, D. Roy, Minor histocompatibility antigens, Blood 76 (1990) 1269–1280.
[14] G. Pietz, R. De, M. Hedberg, V. Sjoberg, O. Sandstrom, O. Hernell, S. Hammarstrom, M.L. Hammarstrom, Immunopathology of childhood celiac disease-key role of intestinal epithelial cells, PLoS ONE 12 (2017) e0185025.
[15] X. Yin, Q. Wang, T. Chen, J. Niu, R. Ban, J. Liu, Y. Mao, C. Pu, CD4+ cells, macrophages, MHC-I and C5b-9 involve the pathogenesis of dysferlinopathy, Int. J. Clin. Exp. Pathol. 8 (2015) 3069–3075.
[16] P.A. Roche, K. Furuta, The ins and outs of MHC class II-mediated antigen processing and presentation, Nat. Rev. Immunol. 15 (2015) 203–216.
[17] Z. Wang, L. Zhang, A. Qiao, K. Watson, J. Zhang, G.H. Fan, Activation of CXCR4 triggers ubiquitination and down-regulation of major histocompatibility complex class I (MHC-I) on epithelioid carcinoma HeLa cells, J. Biol. Chem. 283 (2008) 3951–3959.
[18] R. Busch, C.H. Rinderknecht, S. Roh, A.W. Lee, J.J. Harding, T. Burster, T.M. Hornell, E.D. Mellins, Achieving stability through editing and chaperoning: regulation of MHC class II peptide binding and expression, Immunol. Rev. 207 (2005) 242–260.
[19] J. Imai, H. Hasegawa, M. Maruya, S. Koyasu, I. Yahara, Exogenous antigens are processed through the endoplasmic reticulum-associated degradation (ERAD) in cross-presentation by dendritic cells, Int. Immunol. 17 (2005) 45–53.
[20] J.O. Koopmann, J. Albring, E. Huter, N. Bulbuc, P. Spee, J. Neefjes, G.J. Hammerling, F. Momburg, Export of antigenic peptides from the endoplasmic reticulum intersects with retrograde protein translocation through the Sec61p channel, Immunity 13 (2000) 117–127.
[21] A. Pashine, R. Busch, M.P. Belmares, J.N. Munning, R.C. Doebele, M. Buckingham, G.P. Nolan, E.D. Mellins, Interaction of HLA-DR with an acidic face of HLA-DM disrupts sequence-dependent interactions with peptides, Immunity 19 (2003) 183–192.
[22] S.O. Arndt, A.B. Vogt, S. Markovic-Plese, R. Martin, G. Moldenhauer, A. Wolpl, Y. Sun, D. Schadendorf, G.J. Hammerling, H. Kropshofer, Functional HLA-DM on the surface of B cells and immature dendritic cells, EMBO J. 19 (2000) 1241–1251.
[23] R. Zimmermann, Components and mechanisms of import, modification, folding, and assembly of immunoglobulins in the endoplasmic reticulum, J. Clin. Immunol. 36 (2016) 5–11.
[24] A.B. Vogt, H. Kropshofer, HLA-DM - an endosomal and lysosomal chaperone for the immune system, Trends Biochem. Sci. 24 (1999) 150–154.
[25] J. Qin, C. Mamotte, N.E. Cockett, J.D. Wetherall, D.M. Groth, A map of the class III region of the sheep major histocompatibilty complex, BMC Genomics 9 (2008) 409.
[26] R. Horton, L. Wilming, V. Rand, R.C. Lovering, E.A. Bruford, V.K. Khodiyar, M.J. Lush, S. Povey, C.C. Talbot Jr., M.W. Wright, H.M. Wain, J. Trowsdale, A. Ziegler, S. Beck, Gene map of the extended human MHC, Nat. Rev. Genet. 5 (2004) 889–899.
[27] A. Kumanovics, T. Takada, K.F. Lindahl, Genomic organization of the mammalian MHC, Annu. Rev. Immunol. 21 (2003) 629–657.
[28] R. Dressel, L. Walter, E. Gunther, Genomic and funtional aspects of the rat MHC, the RT1 complex, Immunol. Rev. 184 (2001) 82–95.

[29] S. Beck, J. Trowsdale, The human major histocompatibility complex: lessons from the DNA sequence, Annu. Rev. Genomics Hum. Genet. 1 (2000) 117–137.
[30] A. Blees, D. Januliene, T. Hofmann, N. Koller, C. Schmidt, S. Trowitzsch, A. Moeller, R. Tampe, Structure of the human MHC-I peptide-loading complex, Nature 551 (2017) 525–528.
[31] C. Thomas, R. Tampe, Structure of the TAPBPR-MHC I complex defines the mechanism of peptide loading and editing, Science 358 (2017) 1060–1064.
[32] C. Thomas, R. Tampe, Proofreading of peptide-MHC complexes through dynamic multivalent interactions, Front. Immunol. 8 (2017) 65.
[33] C. Scholz, R. Tampe, The peptide-loading complex–antigen translocation and MHC class I loading, Biol. Chem. 390 (2009) 783–794.
[34] J. Koch, R. Tampe, The macromolecular peptide-loading complex in MHC class I-dependent antigen presentation, Cell. Mol. Life Sci. 63 (2006) 653–662.
[35] P. Cresswell, N. Bangia, T. Dick, G. Diedrich, The nature of the MHC class I peptide loading complex, Immunol. Rev. 172 (1999) 21–28.
[36] T. Elliott, A. Williams, The optimization of peptide cargo bound to MHC class I molecules by the peptide-loading complex, Immunol. Rev. 207 (2005) 89–99.
[37] J. Dissemond, T. Kothen, J. Mors, T.K. Weimann, A. Lindeke, M. Goos, S.N. Wagner, Downregulation of tapasin expression in progressive human malignant melanoma, Arch. Dermatol. Res. 295 (2003) 43–49.
[38] F. Momburg, P. Tan, Tapasin-the keystone of the loading complex optimizing peptide binding by MHC class I molecules in the endoplasmic reticulum, Mol. Immunol. 39 (2002) 217–233.
[39] P.V. Praveen, R. Yaneva, H. Kalbacher, et al., Tapasin edits peptides on MHC class I molecules by accelerating peptide exchange, Eur. J. Immunol. 40 (2010) 214–224.
[40] C. Schneeweiss, M. Garstka, J. Smith, et al., The mechanism of action of tapasin in the peptide exchange on MHC class I molecules determined from kinetics simulation studies, Mol. Immunol. 46 (2009) 2054–2063.
[41] G. Dong, P.A. Wearsch, D.R. Peaper, P. Cresswell, K.M. Reinisch, Insights into MHC class I peptide loading from the structure of the tapasin-ERp57 thiol oxidoreductase heterodimer, Immunity 30 (2009) 21–32.
[42] A. Helenius, M. Aebi, Roles of N-linked glycans in the endoplasmic reticulum, Annu. Rev. Biochem. 73 (2004) 1019–1049.
[43] E.M. Frickel, R. Riek, I. Jelesarov, A. Helenius, K. Wuthrich, L. Ellgaard, TROSY-NMR reveals interaction between ERp57 and the tip of the calreticulin P-domain, Proc. Natl. Acad. Sci. USA 99 (2002) 1954–1959.
[44] E.M. Frickel, P. Frei, M. Bouvier, W.F. Stafford, A. Helenius, R. Glockshuber, L. Ellgaard, ERp57 is a multifunctional thiol-disulfide oxidoreductase, J. Biol. Chem. 279 (2004) 18277–18287.
[45] T.P. Dick, N. Bangia, D.R. Peaper, P. Cresswell, Disulfide bond isomerization and the assembly of MHC class I-peptide complexes, Immunity 16 (2002) 87–98.
[46] D.R. Peaper, P.A. Wearsch, P. Cresswell, Tapasin and ERp57 form a stable disulfide-linked dimer within the MHC class I peptide-loading complex, EMBO J. 24 (2005) 3613–3623.
[47] M. Howarth, A. Williams, A.B. Tolstrup, T. Elliott, Tapasin enhances MHC class I peptide presentation according to peptide half-life, Proc. Natl. Acad. Sci. USA 101 (2004) 11737–11742.
[48] A. Williams, C.A. Peh, T. Elliott, The cell biology of MHC class I antigen presentation, Tissue Antigens 59 (2002) 3–17.
[49] A.P. Williams, C.A. Peh, A.W. Purcell, J. McCluskey, T. Elliott, Optimization of the MHC class I peptide cargo is dependent on tapasin, Immunity 16 (2002) 509–520.
[50] S.M. Rizvi, M. Raghavan, Mechanisms of function of tapasin, a critical major histocompatibility complex class I assembly factor, Traffic 11 (2010) 332–347.
[51] D.R. Peaper, P. Cresswell, Regulation of MHC class I assembly and peptide binding, Annu. Rev. Cell Dev. Biol. 24 (2008) 343–368.
[52] D.R. Peaper, P. Cresswell, The redox activity of ERp57 is not essential for its functions in MHC class I peptide loading, Proc. Natl. Acad. Sci. USA 105 (2008) 10477–10482.
[53] P.A. Wearsch, P. Cresswell, The quality control of MHC class I peptide loading, Curr. Opin. Cell Biol. 20 (2008) 624–631.
[54] D. Stepensky, N. Bangia, P. Cresswell, Aggregate formation by ERp57-deficient MHC class I peptide-loading complexes, Traffic 8 (2007) 1530–1542.
[55] B. Park, S. Lee, E. Kim, K. Cho, S.R. Riddell, S. Cho, K. Ahn, Redox regulation facilitates optimal peptide selection by MHC class I during antigen processing, Cell 127 (2006) 369–382.
[56] E. Rufer, R.M. Leonhardt, M.R. Knittler, Molecular architecture of the TAP-associated MHC class I peptide-loading complex, J. Immunol. 179 (2007) 5717–5727.
[57] G. Niedermann, S. Butz, H.G. Ihlenfeldt, R. Grimm, M. Lucchiari, H. Hoschutzky, G. Jung, B. Maier, K. Eichmann, Contribution of proteasome-mediated proteolysis to the hierarchy of epitopes presented by major histocompatibility complex class I molecules, Immunity 2 (1995) 289–299.
[58] T. Yoshimura, K. Kameyama, T. Takagi, A. Ikai, F. Tokunaga, T. Koide, N. Tanahashi, T. Tamura, Z. Cejka, W. Baumeister, et al., Molecular characterization of the “26S” proteasome complex from rat liver, J. Struct. Biol. 111 (1993) 200–211.
[59] K. Kurokawa, A. Nakano, The ER exit sites are specialized ER zones for the transport of cargo proteins from the ER to the Golgi apparatus, J. Biochem. 165 (2019) 109–114.
[60] K. Kurokawa, M. Okamoto, A. Nakano, Contact of cis-Golgi with ER exit sites executes cargo capture and delivery from the ER, Nat. Commun. 5 (2014) 3653.
[61] S. Cho, J. Ryoo, Y. Jun, K. Ahn, Receptor-mediated ER export of human MHC class I molecules is regulated by the C-terminal single amino acid, Traffic 12 (2011) 42–55.
[62] K.M. Paulsson, M.J. Kleijmeer, J. Griffith, M. Jevon, S. Chen, P.O. Anderson, H.O. Sjogren, S. Li, P. Wang, Association of tapasin and COPI provides a mechanism for the retrograde transport of major histocompatibility complex (MHC) class I molecules from the Golgi complex to the endoplasmic reticulum, J. Biol. Chem. 277 (2002) 18266–18271.
[63] J.W. Yewdell, J.R. Bennink, Immunodominance in major histocompatibility complex class I-restricted T lymphocyte responses, Annu. Rev. Immunol. 17 (1999) 51–88.
[64] D.T. Gillespie, Stochastic simulation of chemical kinetics, Annu. Rev. Phys. Chem. 58 (2007) 35–55.
[65] D.T. Gillespie, M. Roh, L.R. Petzold, Refining the weighted stochastic simulation algorithm, J. Chem. Phys. 130 (2009) 174103.
[66] S. Kundu, Stochastic modelling suggests that an elevated superoxide anion - hydrogen peroxide ratio can drive extravascular phagocyte transmigration by lamellipodium formation, J. Theor. Biol. 407 (2016) 143–154.
[67] A.L. Zarling, C.J. Luckey, J.A. Marto, F.M. White, C.J. Brame, A.M. Evans, P.J. Lehner, P. Cresswell, J. Shabanowitz, D.F. Hunt, V.H. Engelhard, Tapasin is a facilitator, not an editor, of class I MHC peptide binding, J. Immunol. 171 (2003) 5287–5295.
[68] L.C. Simone, C.J. Georgesen, P.D. Simone, X. Wang, J.C. Solheim, Productive association between MHC class I and tapasin requires the tapasin transmembrane/cytosolic region and the tapasin C-terminal Ig-like domain, Mol. Immunol. 49 (2012) 628–639.
[69] E.W. Hewitt, S.S. Gupta, P.J. Lehner, The human cytomegalovirus gene product US6 inhibits ATP binding by TAP, EMBO J. 20 (2001) 387–396.
[70] K. Ahn, A. Gruhler, B. Galocha, T.R. Jones, E.J. Wiertz, H.L. Ploegh, P.A. Peterson, Y. Yang, K. Fruh, The ER-luminal domain of the HCMV glycoprotein US6 inhibits peptide translocation by TAP, Immunity 6 (1997) 613–621.